

Closed-Form Analysis of Squirrel-Cage Induction Motors With Anisotropic Modeling of Stator and Rotor

Layth Qaseer, Sujit Purushothaman, *Student Member, IEEE*, and Francisco de León, *Senior Member, IEEE*

Abstract—This paper presents a closed-form solution of Maxwell's equations in squirrel-cage induction motors. The solution is obtained for a cylindrical multilayer geometry. The squirrel cage is represented by an equivalent anisotropic homogeneous medium. The effect of stator slots and teeth is included by a second anisotropic homogeneous medium. The induction motor is modeled as six concentric cylindrical layers representing the different construction components of the motor. The governing partial differential equations are solved for the excitation source, conducting, and nonconducting regions. The obtained formulas allow for efficient calculations of machine performance which may help the motor designer to select the proper parameters of the machine that fit the design requirements. Accuracy of the method is verified against finite element simulations, a commercial motor design program, and experimental results.

Index Terms—Eddy currents, electromagnetic induction, equivalent circuits, induction motors.

I. INTRODUCTION

ELECTROMAGNETIC fields inside induction motors have been studied before the computer age by several authors; to mention a few we have Hague [1], Smythe [2], and Alger [3]. Because of the lack of computing power, the geometries and excitation conditions did not reflect all the electromagnetic phenomena of a realistic induction motor. As computing power has been made available to engineers, several authors have solved increasingly complex eddy current problems. Good examples include the works of Melcher and Woodson [4], [5], Štafl [6], and Stoll [7]. More recently, we have cited the work of Perry [8] and Tegopoulos [9]. Although the authors in [4]–[9] present solutions to practical eddy current problems, none deals with the cylindrical geometry of a rotating conductive cylinder representing an induction motor.

Multilayer traveling electromagnetic wave problems with the intention of modeling induction motors have been studied by a

number of authors; see, for example, [10]–[14]. Hague [1] and Levi [15] have represented the stator and rotor as fixed current sheets. In [10]–[13], the curvature of the motor is ignored and so is the effect of stator slots. In [14], the cylindrical geometry is considered, but the slots and teeth in both stator and rotor are neglected. In [16], the rotor was allowed to rotate and the stator is represented by a thick conductive layer where eddy currents can be induced. The authors in [17] give an analytical iterative approach with the stator and rotor modeled with anisotropy. A magnetostatic solution was obtained.

This paper presents a 2-D (cylindrical) closed-form solution of the electromagnetic field problem in a three-phase squirrel-cage induction motor considering a model closer to reality than previously published using current sheet representation of the stator and rotor. The rotor is allowed to move. An anisotropic homogeneous representation for both squirrel-cage rotor and stator windings is used. All other regions in the motor are considered nonconducting isotropic media. This field solution to quasi-static problem has not been published earlier, to the authors' knowledge. The incremental contribution is that it accounts for stator impedance, i.e., stator leakage reactance is taken into consideration. Additionally, it accounts for slots and teeth in the stator and the squirrel-cage bars of a moving rotor.

Once a solution to Maxwell's equations is obtained in all regions in terms of the magnetic vector potential, it is possible to compute terminal performance parameters, such as stator impedance, rotor impedance, torque–slip characteristics, rotor losses, air-gap power, output power, etc.

The accuracy of the analytical solution is confirmed by 1) comparing the electromagnetic fields computed analytically against finite element solutions for the same geometry; 2) Computing the output performance of the analytical solution (torque–speed characteristics) and comparing against measurements of a real motor.

II. MATHEMATICAL MODEL

A multilayer traveling wave is usually produced by a polyphase winding, which acts upon a series of laminar regions. A region is defined, for the purpose of this paper, as an area in the motor in which the material can be considered uniform and having boundaries of simple cylindrical shape. When any of the regions is conducting, eddy currents are allowed to be induced and forces tangential to the plane of the region are established.

Manuscript received March 29, 2011; revised June 27, 2011; accepted August 19, 2011. Date of publication May 11, 2012; date of current version July 27, 2012. Paper no. TEC-00159-2011.

L. Qaseer is with the Al-Khwarizmi College of Engineering, University of Baghdad, Baghdad 10071, Iraq, currently he is on a sabbatical leave at the Department of Electrical and Computer Engineering, Polytechnic Institute of New York University, Brooklyn, NY 11201 USA (e-mail: lqaseer@poly.edu).

S. Purushothaman and F. de León are with the Department of Electrical and Computer Engineering, Polytechnic Institute of New York University, Brooklyn, NY 11201 USA (e-mails: sujitp@ieec.org; fdeleon@poly.edu).

Color versions of one or more of the figures in this paper are available online at <http://ieeexplore.ieee.org>.

Digital Object Identifier 10.1109/TEC.2012.2193128

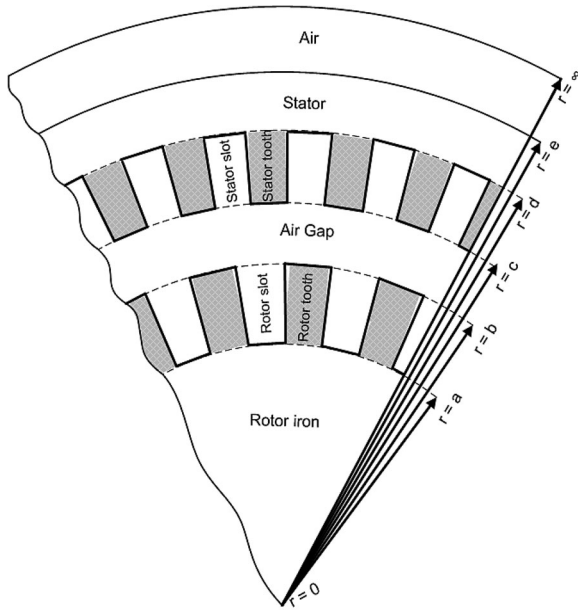


Fig. 1. Regions of the motor represented in the model.

Fig. 1 shows the configuration under study. It consists of a sextant of a motor composed of six concentric cylinders as follows.

- 1) Rotor iron core represented by electrically insulated ferromagnetic laminations of high permeability, $r = [0, a]$.
- 2) Squirrel cage represented by an anisotropic homogeneous material modeling the rotor bars and insulated iron teeth, $r = [a, b]$.
- 3) Air gap, $r = [b, c]$.
- 4) Stator windings modeled as an anisotropic homogeneous material representing slots and insulated iron teeth having a uniform current density excitation, $r = [c, d]$.
- 5) Stator iron core representing by nonconductive ferromagnetic laminations, $r = [d, e]$.
- 6) Exterior (air), $r = [e, \infty)$.

It is further assumed that displacement currents and magnetic saturation are negligible. The analysis is performed using the magnetic vector potential since it yields a 1-D problem with two independent variables.

III. ANISOTROPIC REPRESENTATION OF STATOR AND ROTOR

Due to alternating nature of teeth and slots in the stator and rotor, uniform media used to represent the teeth zones must have different mean permeabilities in a direction parallel with and perpendicular to the air gap as shown in Fig. 2. Furthermore, the slot zones should also represent the conductivity in the direction of current circulation. Fig. 2 represents an anisotropic region. It might be used for a tooth region, a slotted region [11], or a slit solid pole region with copper inserts [18]. The regions considered are composed of wedge shapes. The region is divided into slots of width b and teeth of average width t . The average slot pitch is p_s . The relative radial and circumferential permeabilities μ_r and μ_ϕ , are determined by assuming that in the anisotropic mass the mmf acting in these directions should produce the

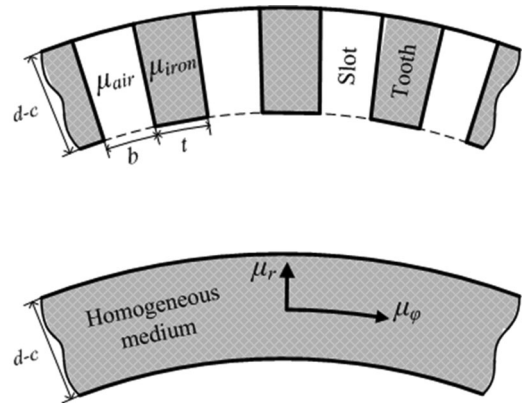


Fig. 2. Representation of slot-tooth region with equivalent anisotropic region.

same flux as it would have produced in the original teeth and slots arrangement.

We can compute the electromagnetic properties of the homogeneous media (for rotor and stator) from the dimensions of the slots and teeth with the following expressions [19] as shown in Fig. 2.

- 1) The equivalent conductivity in the z-direction is

$$\sigma_s = \frac{\sigma_i t + \sigma_c b}{p_s} \quad (1)$$

where σ_s represents the equivalent conductivity of stator winding region. σ_i and σ_c are the conductivities of stator iron core and conducting material, respectively.

- 2) The relative permeability in the radial direction is

$$\mu_r = \frac{b}{p_s} + \mu_i \frac{t}{p_s} \quad (2)$$

where μ_i stands for relative permeability of iron in the tooth region.

- 3) The equivalent relative permeability in the circumferential direction is

$$\mu_\phi = \frac{\mu_i p_s}{\mu_i b + t} \quad (3)$$

It must be noted that μ_r and μ_ϕ are constant in a given region.

IV. THEORETICAL ANALYSIS

It is assumed that the winding produces a perfect sinusoidal traveling wave of electrical frequency ω . The line current density may be represented as

$$J_z = \text{Re}\{J_m e^{j(\omega t - p\phi)}\} \quad (4)$$

where J_m , ω , and p are the amplitude of surface current density, angular frequency, and number of pole pairs, respectively. The current density is given by the total ampere-conductors per cross-sectional area

$$J_m = \frac{6\sqrt{2}NI}{A_s} \quad (5)$$

where N is the effective number of turns per phase, I is the rms value of stator phase current, A_s is the cross-sectional area of stator winding region, and the factor 6 is obtained from the product of three phases and two conductors per turn. The analytical field study is performed considering that the motor is rotating at constant angular speed ω_m . The field produced will link all cylindrical regions from 1 to N . As a first step in the analysis, the magnetic vector potential of a general region is derived. Assuming that all fields vary as $\exp[j(\omega t - p \phi)]$ and omitting this factor from all field expressions that follow, Maxwell's equations for any region in the model are

$$\nabla \times \bar{H} = \bar{J} \quad (6)$$

$$\nabla \times \bar{E} = -\frac{\partial \bar{B}}{\partial t} \quad (7)$$

with

$$\bar{B} = \mu \bar{H} \quad (8)$$

and

$$\bar{J} = \sigma \bar{E}. \quad (9)$$

Ohm's law for a medium moving with velocity $\omega_m r$ in [meter/second] is

$$\bar{J} = \sigma(\bar{E} + \omega_m r \times \bar{B}). \quad (10)$$

\bar{J} in the aforementioned equations represents either the impressed current density or the induced current density. Using the fact that $\nabla \cdot \bar{B} = 0$, we define the magnetic vector potential \bar{A} as

$$\bar{B} = \nabla \times \bar{A} \quad (11)$$

such that the identity $\nabla \cdot (\nabla \times \bar{A}) = 0$ is satisfied.

Using (6), (8), (10), and (11), we obtain the following general partial differential equation:

$$\frac{\partial^2 A_z}{\partial r^2} + \frac{1}{r} \frac{\partial A_z}{\partial r} + \frac{1}{r^2} \frac{\mu_\phi}{\mu_r} \frac{\partial^2 A_z}{\partial \phi^2} = -\mu_0 \mu_\phi J_z. \quad (12)$$

Insulated laminations in the rotor and stator core are considered by setting the conductivity to zero (neglecting the eddy currents) for these regions. Hence, for the zero conductivity regions such as rotor core, air gap, stator core, and exterior, we need to solve Laplace's equation $\nabla^2 A_z = 0$ which reduces to

$$\frac{\partial^2 A_z}{\partial r^2} + \frac{1}{r} \frac{\partial A_z}{\partial r} + \frac{1}{r^2} \frac{\partial^2 A_z}{\partial \phi^2} = 0. \quad (13)$$

The aforementioned equation is solved using separation of variables. Consequently, the solution is the product of two functions of only one variable $A(r, \phi) = R(r)\Phi(\phi)$. Because of symmetry, we know that the variation as a function of ϕ should be $e^{-jp\phi}$. The function $R(r)$ can be obtained by the solution of Euler equation for (13) given by

$$\frac{d^2 R(r)}{dr^2} + \frac{1}{r} \frac{dR(r)}{dr} - \frac{p^2}{r^2} \frac{d^2 R(r)}{d\phi^2} = 0 \quad (14)$$

and the general solution is given by

$$A_3 = c_1 r^{-p} + c_2 r^p \quad (15)$$

where c_1 and c_2 are arbitrary constants.

For the stator winding region, the complete solution of (12) is the sum of the solution of Laplace's equation and the particular integral which is given by

$$A_z = c_1 r^{-v} + c_2 r^v - \frac{\mu_0 \mu_\phi J_m}{(4 - p^2(\mu_\phi/\mu_r))} r^2 \quad (16)$$

where

$$v = p \sqrt{\frac{\mu_\phi}{\mu_r}} \quad (17)$$

and for the squirrel cage of high conductivity material, we have the following differential equation:

$$\frac{\partial^2 A_z}{\partial r^2} + \frac{1}{r} \frac{\partial A_z}{\partial r} + \frac{1}{r^2} \frac{\mu_\phi}{\mu_r} \frac{\partial^2 A_z}{\partial \phi^2} = -\mu_0 \mu_\phi \sigma (-j\omega A_z + jp\omega_m A_z) \quad (18)$$

where ω_m and σ are the rotor mechanical speed in [radian/second] and squirrel-cage conductivity in [Siemens per meter], respectively. Defining the slip $s = (\omega - p\omega_m)/\omega$, the aforementioned equation reduces to the following modified Bessel equation:

$$r^2 \frac{d^2 R(r)}{dr^2} + r \frac{dR(r)}{dr} - (v^2 + \alpha^2 r^2) R(r) = 0 \quad (19)$$

where

$$\alpha^2 = js\omega\mu_0\mu_\phi\sigma. \quad (20)$$

The complete solution for the squirrel-cage region is given by

$$A_z = c_1 I_v(\alpha r) + c_2 K_v(\alpha r) \quad (21)$$

where I_v and K_v are the modified Bessel's function of the first kind and second kind, respectively, of order v . Thus, for the six regions in Fig. 1, we obtain the following set of solutions for the magnetic vector potential.

1) Rotor iron core

$$A_1 = c_{12} r^p. \quad (22)$$

2) Squirrel cage

$$A_2 = c_{21} I_v(\alpha r) + c_{22} K_v(\alpha r). \quad (23)$$

3) Air gap

$$A_3 = c_{31} r^{-p} + c_{32} r^p. \quad (24)$$

4) Stator winding

$$A_4 = c_{41} r^{-v} + c_{42} r^v - \frac{\mu_0 \mu_\phi J_m}{(4 - p^2(\mu_\phi/\mu_r))} r^2. \quad (25)$$

5) Stator iron core

$$A_5 = c_{51} r^{-p} + c_{52} r^p. \quad (26)$$

6) Exterior

$$A_6 = c_{61} r^{-p}. \quad (27)$$

Constants c_{ij} in (22)–(27) will be computed from the boundary conditions. We have already omitted c_{11} and c_{62} because for $r = 0$ and $r = \infty$, the field should vanish. For the remaining constants, we use the following boundary conditions:

$$\begin{aligned} B_{r_i} &= B_{r_{i+1}} \\ H_{\phi_i} &= H_{\phi_{i+1}}. \end{aligned} \quad (28)$$

Combining the two expressions in (28) with (22)–(27), we write a set of ten linear algebraic equations where the unknowns are the constants c_{ij} yielding to the following band matrix equation:

$$Mc = b \quad (29)$$

where the matrix M , and the vectors c and b along with their elements are given in the Appendix. Once c_{ij} are known, the magnetic vector potential \bar{A} is known in all regions. Then, analytical expressions for the magnetic flux density components can be obtained using (11) for each specific region, namely the radial component B_r and the circumferential component B_ϕ . Using (8), we can compute the magnetic field strength \bar{H} and the rotor-induced current density is calculated from (6) as

$$\begin{aligned} \bar{J} &= -\frac{\alpha^2}{\mu_0 \mu_{\phi_2}} \bar{A} \\ &= -\frac{\alpha^2}{\mu_0 \mu_{\phi_2}} [c_{21} I_v(\alpha r) + c_{22} K_v(\alpha r)]. \end{aligned} \quad (30)$$

The air-gap power P_g is calculated through the concept of Poynting vector

$$P_g = \frac{1}{2} \operatorname{Re} \int_s (\bar{E} \times \bar{H}^*) \cdot d\bar{S} \quad (31)$$

where the integration is carried out over a cylindrical surface passing through the air gap.

The rotor losses P_r can also be obtained from the relation

$$P_r = \frac{1}{2\sigma} \int_V (\bar{J} \cdot \bar{J}^*) dV \quad (32)$$

where the integration is carried throughout the squirrel-cage volume. The force density \bar{F} in Newton per cubic meter is given by

$$\bar{F} = \frac{1}{2} \operatorname{Re} \{ \bar{J} \times \bar{B}^* \}. \quad (33)$$

The circumferential force density F_ϕ that is responsible for producing the torque is given by the following expression:

$$F_\phi = \frac{p}{r \mu_0 \mu_{\phi_2}} |\alpha [c_{21} I_v(\alpha r) + c_{22} K_v(\alpha r)]|^2. \quad (34)$$

The torque produced (T) is obtained from

$$T = \int_V r F_\phi dV \quad (35)$$

where the integration is carried throughout the total volume of the squirrel cage giving the following expression:

$$T = \int_0^l \int_0^{2\pi} \int_a^b \frac{p |\alpha [c_{21} I_v(\alpha r) + c_{22} K_v(\alpha r)]|^2}{2\mu_0 \mu_{\phi_2}} r dr d\phi dz \quad (36)$$

where l is the axial length of the motor. The motor output power P_o is then obtained from

$$P_o = \omega_m T \quad (37)$$

which should be equivalent to the value obtained from the relation $P_o = (1 - s)P_g$.

The power delivered by the source P_s is given by [20]

$$P_s = -\frac{1}{2} \operatorname{Re} \int_V (\bar{E} \cdot \bar{J}^*) dV \quad (38)$$

where the integration is carried throughout the entire volume of the stator winding region. J^* represents the conjugate of J . The stator copper loss P_c is calculated from

$$P_c = \frac{1}{2\sigma_4} \int_V (\bar{J} \cdot \bar{J}^*) dV \quad (39)$$

where σ_4 refers to the conductivity of stator winding region.

The induced voltage in the stator E_s that accounts for cross-gap flux as well as slots and other leakages is obtained from the relation

$$3E_s I^* = -\frac{1}{2} \int_V (\bar{E} \cdot \bar{J}^*) dV \quad (40)$$

where the integration is carried throughout the volume of stator winding region. The input impedance Z_{in} as seen by the stator is given by

$$Z_{in} = \frac{E_s}{I}. \quad (41)$$

Alternatively, the input impedance may be calculated from the flux linking the stator winding [21]

$$Z_{in} = \frac{j2\pi\sqrt{2}\omega l N}{IA_s} \int_c^d A r dr. \quad (42)$$

For further verification of the computational results, it is interesting to note that the torque acting on the stator T_s can be calculated by integrating the circumferential force density throughout the volume of stator winding region as

$$T_s = \frac{1}{2} \operatorname{Re} \int_0^l \int_0^{2\pi} \int_c^d \{J_z B_r^*\} r^2 dr d\phi dz \quad (43)$$

which should be opposite in sign with that obtained from (36).

V. EQUIVALENT CIRCUIT PARAMETERS

The equivalent circuit parameters have been extensively used by designers and analysts to study the performance characteristics of induction machines. This section gives another method of calculating equivalent circuit parameters and creates a link between the analytical model presented here and the Steinmetz equivalent circuit.

The leakage and magnetizing reactances are found by performing the locked rotor and no-load tests, respectively. Similarly, the leakage and magnetizing reactances can be found using the magnetic energy stored at standstill and synchronous speed, respectively. This is equivalent to performing the tests on the machine.

For $\omega_m = 0$, we have

$$\begin{aligned} 3L_1 I^2 &= \frac{1}{2} \int_V (\bar{B} \cdot \bar{H}^*) dV \\ &= \frac{1}{2} \mu_0 \int_0^l \int_0^{2\pi} \int_c^d (\mu_r |H_r|^2 + \mu_\phi |H_\phi|^2) r dr d\phi dz \end{aligned} \quad (44)$$

$$\begin{aligned} 3L_2 I^2 &= \frac{1}{2} \int_V (\bar{B} \cdot \bar{H}^*) dV \\ &= \frac{1}{2} \mu_0 \int_0^l \int_0^{2\pi} \int_a^b (\mu_r |H_r|^2 + \mu_\phi |H_\phi|^2) r dr d\phi dz \end{aligned} \quad (45)$$

and for $\omega_m = \omega/p$, we have

$$3L_m I^2 = \frac{1}{2} \mu_0 \int_0^l \int_0^{2\pi} \int_b^c (|H_r|^2 + |H_\phi|^2) r dr d\phi dz \quad (46)$$

where L_1 , L_2 and L_m are the stator leakage, rotor leakage, and magnetizing air-gap inductances, respectively.

Analogous to the method followed to calculate the rotor resistance from the blocked rotor test, the rotor resistance r_2 is calculated from

$$P_r = 3I^2 r_2. \quad (47)$$

The stator resistance r_1 is calculated from

$$P_c = 3I^2 r_1. \quad (48)$$

VI. RESULTS

The electromagnetic field solution for a three-phase induction motor using the homogeneous medium representation for both stator and rotor is validated in four ways. 1) Using a commercial finite element program (Comsol Multiphysics [22]), 2) comparing the output performance (torque–speed characteristics) against the results of a professional grade motor design program (RMxpert [23]), 3) comparing with a load test on a real motor whose data are given in Table I, and 4) comparing with the torque–speed curve obtained from the conventional equivalent circuit method, where the parameters have been obtained from the locked rotor and no-load tests.

Fig. 3 shows the finite element discretization of the model. Although with finite element method (FEM) one can solve a more realistic geometrical configuration, FEM is used here for the purpose of validating the analytical solution; therefore, we use the same arrangement as in Fig. 1. It should be noted that the air-gap layer is not clearly visible in Fig. 3 since the drawing is made to scale.

Fig. 4 compares the distribution of the rotor-induced current density calculated with FEM and the proposed model (30) for

TABLE I
MACHINE DATA

Manufacturer	Westinghouse
Frame	K56H
Rated power, (hp)	0.75
Number of poles	4
Line stator voltage, (V)	230/460
Rated stator current, (A)	2.4/1.2
Number of turns per phase	342
Frequency, (Hz)	60
Rated speed, (rpm)	1725
Rotor core radius, a (mm)	33.6
Outer rotor radius, b (mm)	48.2
Inner stator radius, c (mm)	48.5
Outer stator winding radius, d (mm)	68
Outer stator iron radius, e (mm)	81
Relative permeability of iron (RM 23)	3800
Rotor bar conductivity, (S/m)	1.5×10^7

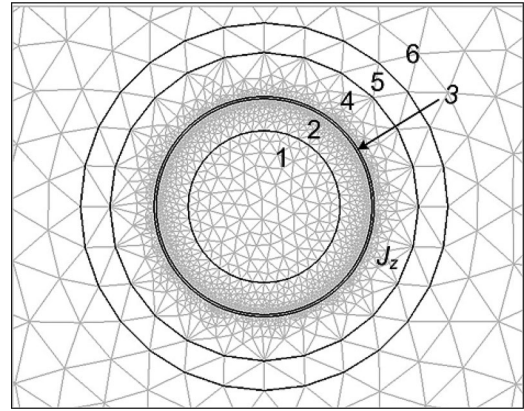


Fig. 3. Finite element discretization of the model.

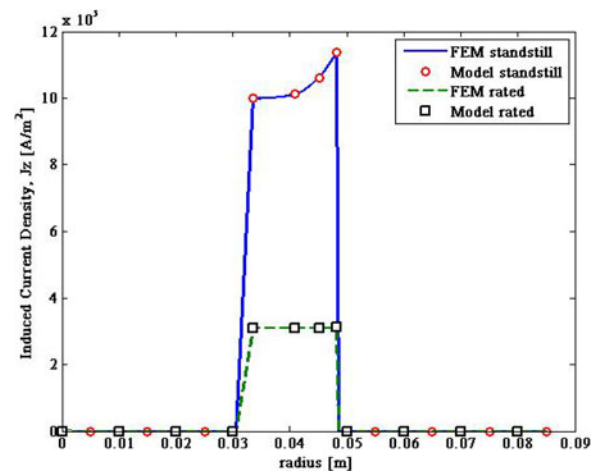


Fig. 4. Comparison of induced current density computed from FEM and proposed model.

standstill and rated speed. One can appreciate that the two solutions are identical. At standstill, the induced currents in the squirrel cage are at rated frequency, hence inducing large eddy currents. The current distribution is not uniform showing the typical characteristic skin effect (larger current density near the external surface). At rated speed, the induced currents are almost

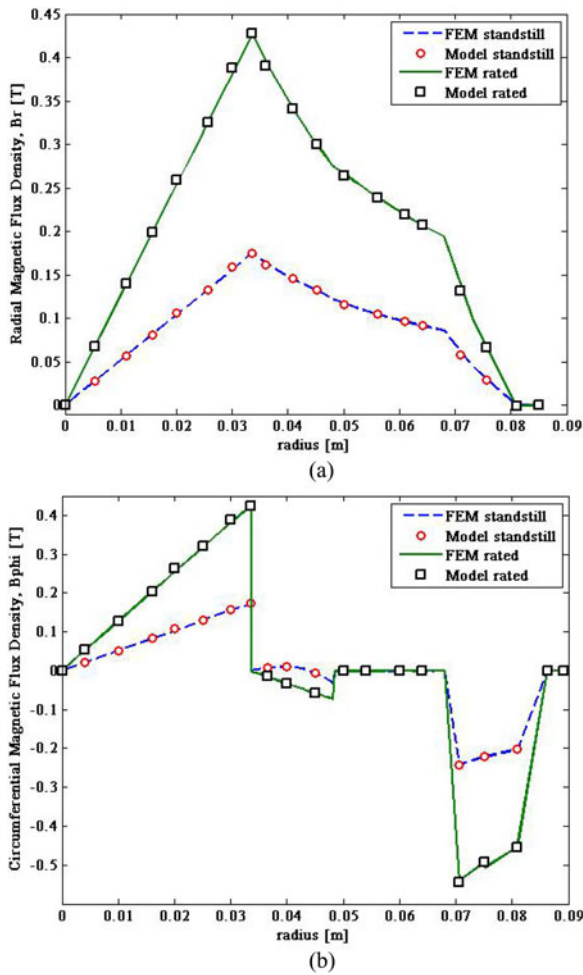


Fig. 5. Comparison of flux density components computed from FEM and proposed model. (a) Radial component. (b) Circumferential component.

uniformly distributed consistent with the expected response for very low frequency induced current.

Fig. 5(a) and (b) presents the magnetic flux density (radial and circumferential components) from FEM and the model for standstill and rated speed conditions. One can appreciate that the magnitude of the flux density at rated speed is substantially larger than at standstill. This is because at standstill, most of the flux is due to armature reaction (leakage flux), while at rated speed the magnetizing component is dominant. This is better illustrated in the following with Figs. 6 and 7.

Figs. 6 and 7 show the flux contours at standstill and rated speed, respectively. It can be observed that at rated speed, the flux in the rotor and stator penetrates the core, while at standstill the flux concentrates in the region around the air gap. This is caused by the power frequency currents induced in the rotor at standstill. The penetration of the flux in the squirrel cage is limited by the skin depth. At rated speeds, since the frequency of induced currents is very low (slip frequency ≈ 0), the flux is able to penetrate the squirrel cage into the rotor iron core. This is made evident by comparing the number of flux lines in the rotor core in Figs. 6 and 7. The large magnetizing flux is the

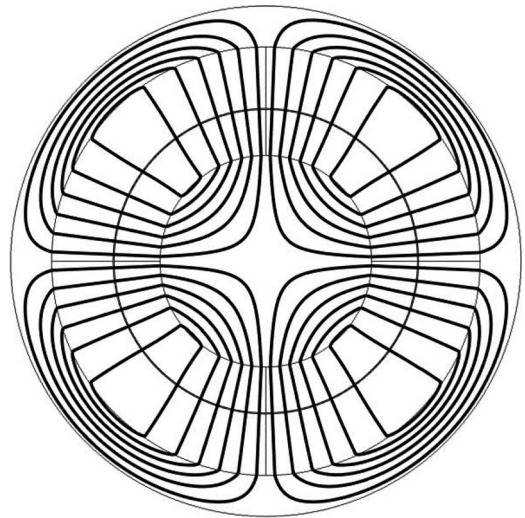


Fig. 6. Magnetic flux density contours at rated speed.

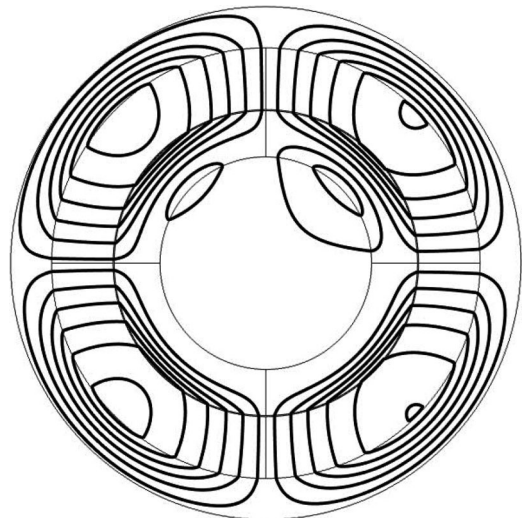


Fig. 7. Magnetic flux density contours at standstill.

primary reason for the magnetizing reactance to be very large as compared to the leakage reactance.

Fig. 8 compares the torque–speed characteristic for the following four cases.

- 1) The conventional equivalent circuit based on standard tests, i.e., the blocked rotor test and no-load test.
- 2) A load tests on real motor load, i.e., the motor is loaded slowly from no-load (speed near synchronous) to the breakdown torque.
- 3) The motor designed with RMxpert, a production grade computer software [23], which works based on the equivalent reluctance network to obtain the equivalent circuit.
- 4) The plot obtained using the proposed model of this paper.

One can appreciate that the four curves match relatively well between each other. In the operating region, the behavior of the analytical model of this paper is almost identical to the load test measurements and the simulation with the standard equivalent circuit. The breakdown torque and the slip at which it occurs are

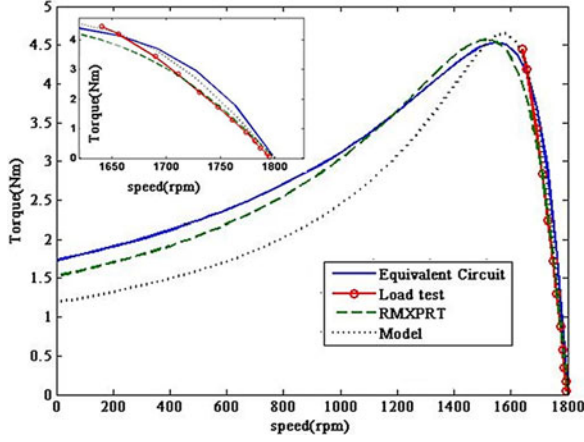


Fig. 8. Comparison of torque–speed characteristics for the following cases: equivalent circuit from the standard tests, load test results, RMXprt model, and proposed model in this paper.

also in relatively good agreement with the experimental results. This is an indication that the leakage inductance and the total resistance are properly computed with the model.

One can note that the model derived from RMXprt gives slightly worse results than our model in the operating region and somewhat better results for the starting torque.

The differences for the starting torque are attributed to the following factors. 1) The approximation made by substituting the actual slot-teeth geometry of the stator and rotor by anisotropic media, which is more important at large slips; 2) the use of constant permeabilities in both directions rather than varying permeabilities with position; 3) the proposed model does not consider nonlinearities; and 4) the lack of precision in the measurement of the geometrical dimensions of the motor.

Performance parameters can be drawn from the model of this paper in addition to the distribution of the electromagnetic fields inside the machine: torque–speed characteristics, stator and rotor losses, input, air gap and output power, induced voltage, input power factor, and efficiency.

The model of this paper can be extended to consider saturation by incorporating an iterative approach within the analytical model by numerically varying the value of μ .

VII. CONCLUSION

A closed-form solution for the electromagnetic fields inside a three-phase squirrel-cage induction motor has been presented. The solution has been obtained by representing the motor by a cylindrical multilayer geometry. Both the squirrel cage and the slots teeth of the stator have been modeled by equivalent anisotropic homogeneous media. The correctness of the obtained analytical expressions has been corroborated by finite element simulations using the same cylindrical geometry.

The applicability of the solution has been established by comparing the calculated torque–speed characteristics against tests performed on a real motor. Since the model is noniterative, the formulas of this paper offer a fast and efficient alternative for field computations in induction motors. Parametric analyses, varying the number of poles, rotor conductivity, air-gap length,

and squirrel-cage thickness, can be performed to help the designer meet the design objectives and constraints.

APPENDIX

Elements of the matrix equation $Mc = b$.

1) The constant vector c :

$$c = [c_{12} c_{21} c_{22} c_{31} c_{32} c_{41} c_{42} c_{51} c_{52} c_{61}]^T. \quad (49)$$

2) The excitation vector b :

$$b = \left[0, 0, 0, 0, -\frac{\mu_0 \mu_{\phi_4} J_m c^2}{(4 - p^2(\mu_{\phi_4}/\mu_{r_4}))}, -\frac{2\mu_0 J_m c}{(4 - p^2(\mu_{\phi_4}/\mu_{r_4}))}, \frac{\mu_0 \mu_{\phi_4} J_m d^2}{(4 - p^2(\mu_{\phi_4}/\mu_{r_4}))}, \frac{2\mu_0 J_m d}{(4 - p^2(\mu_{\phi_4}/\mu_{r_4}))}, 0, 0 \right]^T. \quad (50)$$

3) The coefficient square matrix M :

$$\begin{aligned} m_{11} &= a^p, & m_{12} &= -I_v(\alpha a), & m_{13} &= -K_v(\alpha a) \\ m_{21} &= \frac{pa^{p-1}}{\mu_{\phi_1}}, & m_{22} &= \frac{\alpha I'_v(\alpha a)}{2\mu_{\phi_2}}, & m_{23} &= \frac{\alpha K'_v(\alpha a)}{2\mu_{\phi_2}} \\ m_{32} &= I_v(\alpha b), & m_{33} &= K_v(\alpha b), & m_{34} &= -b^{-p}, \\ m_{35} &= -b^p \\ m_{42} &= \frac{\alpha I'_v(\alpha b)}{2\mu_{\phi_2}}, & m_{43} &= \frac{\alpha K'_v(\alpha b)}{2\mu_{\phi_2}}, & m_{44} &= pb^{-p-1}, \\ m_{45} &= -pb^{p-1} \\ m_{54} &= c^{-p}, & m_{55} &= c^p, & m_{56} &= -c^{-v}, & m_{57} &= -c^v \\ m_{64} &= -pc^{-p-1}, & m_{65} &= pc^{p-1}, & m_{66} &= \frac{vc^{-v-1}}{\mu_{\phi_4}}, \\ m_{67} &= -\frac{vc^{v-1}}{\mu_{\phi_4}} \\ m_{76} &= d^{-v}, & m_{77} &= d^v, & m_{78} &= -d^{-p}, & m_{79} &= -d^p \\ m_{86} &= -\frac{vd^{-v-1}}{\mu_{\phi_4}}, & m_{87} &= \frac{vd^{v-1}}{\mu_{\phi_4}}, & m_{88} &= \frac{pd^{-p-1}}{\mu_{\phi_5}}, \\ m_{89} &= -\frac{pd^{p-1}}{\mu_{\phi_5}} \\ m_{98} &= e^{-p}, & m_{99} &= e^p, & m_{910} &= -e^{-p} \\ m_{108} &= -\frac{pe^{-p-1}}{\mu_{\phi_5}}, & m_{109} &= \frac{pe^{p-1}}{\mu_{\phi_5}}, & m_{1010} &= pe^{-p-1}. \end{aligned} \quad (51)$$

ACKNOWLEDGMENT

The authors would like to thank Prof. J. Rogers of the Department of Mathematics, New York University, for valuable help and advice. The authors would also like to thank S. Brahma and A. Sharma for performing practical tests.

REFERENCES

- [1] B. Hague, *Electromagnetic Problems in Electrical Engineering*. London, U.K.: Oxford Univ. Press, 1929.
- [2] W. R. Smythe, *Static and Dynamic Electricity*. New York: McGraw-Hill, 1950.
- [3] P. L. Alger, *The Nature of Polyphase Induction Machines*. New York: Wiley, 1951.
- [4] J. R. Melcher and H.H. Woodson, *Electromechanical Dynamics*. New York: Wiley, 1968.
- [5] J. R. Melcher, *Continuum Electromechanics*. Cambridge, MA: MIT Press, 1981.
- [6] M. Štafl, *Electrodynamics of Electrical Machines*. Prague, Czechoslovakia: Academia, 1967.
- [7] R. L. Stoll, *The Analysis of Eddy Currents*. London, U.K.: Oxford Univ. Press, 1974.
- [8] M. P. Perry, *Low Frequency Electromagnetic Design*. New York: Marcel Dekker, 1985.
- [9] J. A. Tegopoulos, *Eddy Currents in Linear Conducting Media*. New York: Elsevier, 1985.
- [10] E. Mishkin, "Theory of the squirrel-cage induction motor derived directly from Maxwell's field equations," *Quart. J. Mech. Appl. Math.*, vol. 7, pp. 472–487, 1954.
- [11] A. L. Cullen and T. H. Barton, "A simplified electromagnetic theory of the induction motor using the concept of wave impedance," *Proc. IEE C, Monographs*, vol. 105, pp. 331–336, 1958.
- [12] J. C. Wilson, E. A. Erdelyi, and R. E. Hopkins, "Aerospace composite-rotor induction motors," *IEEE Trans. Aerosp.*, vol. AES-3, no. 2, pp. 18–23, Jun. 1965.
- [13] J. C. West and D. E. Hesmondhalgh, "The analysis of thick-cylinder induction machines," *Proc. IEE C, Monographs*, vol. 109, pp. 172–181, 1962.
- [14] L. S. Piggott, "A theory of the operation of cylindrical induction motors with squirrel-cage rotors," *Proc. IEE C, Monographs*, vol. 109, pp. 270–282, 1962.
- [15] E. Levi, *Polyphase Motors: A Direct Approach to their Design*. New York: Wiley, 1984.
- [16] E. Bernal-Luna, "Analysis of the electromagnetic field inside of an induction motor and its application to the study of the starting and short circuit transients," M.S. Thesis, Dept. Electr. Eng., Instituto Politecnico Nacional, Mexico City, Mexico, Feb. 1996.
- [17] I. Boldea and S. A. Nasar, *The Induction Machines Design Handbook*, 2nd ed. Boca Raton: CRC Press, 2009.
- [18] K. R. Dorairaj and M. R. Krishnamurthy, "Polyphase induction machines with slitted ferromagnetic rotor," *IEEE Trans. Power App. Syst.*, vol. PAS-86, no. 7, pp. 835–855, Jul. 1967.
- [19] E. M. Freeman, "Traveling waves in induction machines: Input impedance and equivalent circuits," *Proc. IEE*, vol. 115, no. 12, pp. 1772–1776, 1968.
- [20] R. M. Fano, L. J. Chu, and R. B. Adler, *Electromagnetic Fields, Energy and Forces*. New York, Wiley, 1963, p. 323.
- [21] T. Miyoshi, M. Sumiya, and H. Omori, "Analysis of an induction heating system by the finite element method combined with a boundary integral equation," *IEEE Trans. Magn.*, vol. MAG-23, no. 2, pp. 1827–1832, Mar. 1987.
- [22] Comsol Multiphysics, ACDC Module User's Guide, Comsol AB Group, Burlington, MA, pp. 1–222, 2010.
- [23] Ansoft RMxprt (2011). [Online]. Available: <http://www.ansoft.com/products/em/rmxprt>



Layth Qaseer received the B.Sc., M.Sc., and Ph.D. degrees from the University of Baghdad, Baghdad, Iraq, in 1979, 1993, and 2004, respectively, all in electrical engineering.

During 1979–2001, he was at National Scientific Research Center and the Ministry of Industry. In 2005, he joined Al-Khwarizmi College of Engineering, University of Baghdad, Baghdad, Iraq, where he is currently on a sabbatical leave from the Department of Electrical and Computer Engineering, Polytechnic Institute of New York University, Brooklyn. His research interests include rotary, flat linear, tubular linear and helical motion induction motors as well as induction heating systems.



Sujit Purushothaman (S'09) received the B.E. degree in electrical engineering from the Sardar Patel College of Engineering, Mumbai University, Mumbai, India, in 2005, and the Master's degree in electrical engineering from Polytechnic Institute of New York University, Brooklyn, NY, in 2009. He is currently working toward the Ph.D. degree at the Polytechnic Institute of New York University, Brooklyn.

His work experience includes testing and development of medium voltage switchgear for Siemens India. His research interests include power system transients, subsynchronous resonance damping, machine design, and modeling and thermal modeling of electrical machines.



Francisco de León (S'86–M'92–SM'02) received the B.Sc. and M.Sc. (Hons.) degrees in electrical engineering from the National Polytechnic Institute, Mexico City, Mexico, in 1983 and 1986, respectively, and the Ph.D. degree from the University of Toronto, Toronto, ON, Canada, in 1992.

He has held several academic positions in Mexico and was with the Canadian electric industry. He is currently an Associate Professor at the Polytechnic Institute of New York University, Brooklyn. His research interests include the analysis of power definitions under nonsinusoidal conditions, the transient and steady-state analyses of power systems, the thermal rating of cables and transformers, and the calculation of electromagnetic fields applied to machine design and modeling.